

World-VLA-Loop: Closed-Loop Learning of Video World Model and VLA Policy

Xiaokang Liu ^{*1} Zechen Bai ^{*1} Hai Ci ¹ Kevin Yuchen Ma ¹ Mike Zheng Shou ^{†1}

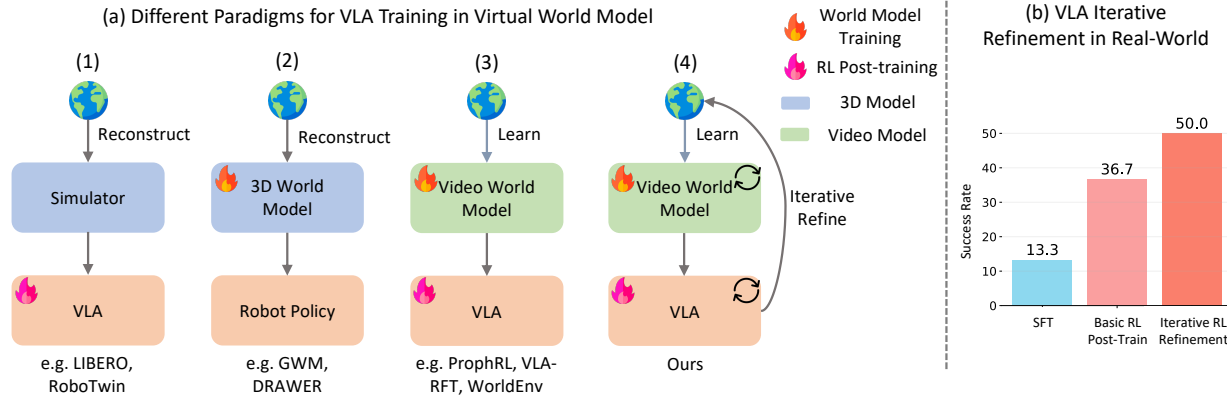


Figure 1. (a) Paradigms for world-model-based VLA reinforcement learning. Comparison of existing methodologies: current approaches typically rely on reconstructing the environment within 3D world or training video world models that simulate the environment. To address the imprecise action-following inherent in existing video-based simulators, we propose World-VLA-Loop, a closed-loop paradigm that jointly optimizes the world model and the VLA policy to iteratively enhance the performance and grounding of both. (b) We show that the real-world policy success rate is improved by 36.7% after two iterations of joint optimization with VLA model and world model.

Abstract

Recent progress in robotic world models has leveraged video diffusion transformers to predict future observations conditioned on historical states and actions. While these models can simulate realistic visual outcomes, they often exhibit poor action-following precision, hindering their utility for downstream robotic learning. In this work, we introduce World-VLA-Loop, a closed-loop framework for the joint refinement of world models and Vision-Language-Action (VLA) policies. We propose a state-aware video world model that functions as a high-fidelity interactive simulator by jointly predicting future observations and reward signals. To enhance reliability, we introduce the SANS dataset, which incorporates near-success trajectories to improve action-outcome alignment within the world model. This framework enables a closed-loop for reinforcement learning (RL) post-training of VLA policies en-

tirely within a virtual environment. Crucially, our approach facilitates a co-evolving cycle: failure rollouts generated by the VLA policy are iteratively fed back to refine the world model's precision, which in turn enhances subsequent RL optimization. Evaluations across simulation and real-world tasks demonstrate that our framework significantly boosts VLA performance with minimal physical interaction, establishing a mutually beneficial relationship between world modeling and policy learning for general-purpose robotics. Project page: <https://showlab.github.io/World-VLA-Loop/>.

1. Introduction

Vision-Language-Action (VLA) models have emerged as a dominant paradigm for robotic manipulation by leveraging large language model priors to map natural language directly to low-level control (Black et al., 2024; Kim et al., 2024; 2025; Liu et al., 2025). To improve generalization, recent works (Lu et al., 2025a; Li et al., 2025b; Intelligence et al., 2025) have integrated reinforcement learning (RL) to refine policies through interaction, enabling agents to re-

^{*}Equal contribution [†]Correspondence author. ¹Show Lab, National University of Singapore. Correspondence to: Mike Zheng Shou <mike.zheng.shou@gmail.com>.



Figure 2. Current world models struggle to accurately simulate failure cases stemming from minor action errors. This is primarily due to their inability in modeling fine-grained interaction dynamics and precise action conditioning. In the figure, the transparent overlays denote the ground-truth gripper trajectories, illustrating cases where the robot fails to grasp the object.

cover from suboptimal actions without requiring additional expert demonstrations. Despite this potential, existing RL post-training remains largely confined to simulated environments (Liu et al., 2023; Tao et al., 2024) because real-world RL is prohibitively expensive. Specifically, the high sample complexity of RL necessitates thousands of physical rollouts, which requires constant human supervision for resets, and risks safety-critical failures during the exploration.

As shown in Figure 1, a promising approach to overcoming real-world RL challenges involves developing world models as virtual environments, which we categorize into three major paradigms: (1) **Handcrafted digital twins** (Liu et al., 2023; Chen et al., 2025b), which rely on manual asset creation and physics engine modeling but often lack the photorealism and physical fidelity required for real-world adaptation; (2) **3D-based reconstruction** (Lu et al., 2025b; Xia et al., 2025), which utilize geometric 3D methods to represent scenes but struggle to generalize across diverse environments and rarely support stochastic exploration; and (3) **Action-conditioned video world models** (Zhang et al., 2025; Li et al., 2025a; Xiao et al., 2025), which leverage pretrained priors for better generalization but suffer from imprecise action-following and ungrounded reward signals. In these models, poor fidelity to action conditioning causes predicted trajectories to diverge from actual execution outcomes. As shown in Figure 2, existing models such as Cosmos-Predict 2 (Ali et al., 2025) frequently hallucinate successful outcomes even when provided with erroneous actions, suggesting a reliance on visual priors over underlying physical dynamics. This lack of precise action following makes existing video world models unreliable as reward functions for effective RL deployment.

To address the limitations of imprecise action-following and unreliable reward signals in existing robotic world models, we propose World-VLA-Loop, trying to address these challenges through two distinct layers. At the algorithmic level, we establish a co-evolving paradigm motivated by the observation that VLA behaviors shift during training. To ensure the broad coverage of these changing states, the world model first facilitates RL post-training for the VLA

policy; subsequently, the failure rollouts generated by the updated policy are fed back to refine the world model to provide more robust action-following observation and reward. Supporting this framework at the architectural level, we introduce the SANS dataset, which incorporates both successful and near-success trajectories, to sharpen the model’s action-outcome alignment. Trained on this data, our state-aware video world model serves as a high-fidelity virtual environment by jointly predicting future observations and rewards. Our contributions are summarized as follows:

- We introduce World-VLA-Loop, a closed-loop framework that establishes a co-evolving cycle between world model and VLA policy learning through a novel iterative refinement paradigm.
- We develop a state-aware world model that achieves superior action-following precision by combining joint reward-and-video supervision on diffusion latents with curated near-success trajectories. These designs enable high-fidelity, action-conditioned prediction of both execution outcomes and intrinsic rewards.
- We conduct evaluations on the LIBERO benchmark (Liu et al., 2023) and real-world settings, demonstrating that World-VLA-Loop significantly improves VLA performance across simulation and physical scenarios while reducing the necessity for costly real-world interactions.

2. Related Work

2.1. VLA Models for Robot Manipulation

By leveraging the intelligence and strong prior knowledge of foundation VLMs, VLA has emerged as a mainstream paradigm for robot manipulation. Pretrained VLMs offer strong generalization capabilities and are typically fine-tuned on robotic demonstration data to adapt to action spaces (Driess et al., 2023; Karamcheti et al., 2024). Most existing VLA methods follow a two-stage pipeline: the VLM first produces high-level action tokens, which are then refined by a diffusion head or other sub-modules to generate precise low-level control actions (Kim et al., 2024; 2025; Black et al., 2024). However, the dominant training paradigm remains imitation learning, which suffers from data scarcity and compounding errors at test time, ultimately limiting generalization.

Recently, inspired by advances in reinforcement learning for language models, exemplified by Group Relative Policy Optimization (GRPO) (Shao et al., 2024), there has been growing interest in refining VLA policies through RL-based post-training. VLA-RL (Lu et al., 2025a) introduces a learned reward model to provide dense trajectory feedback, while SimpleVLA-RL (Li et al., 2025b) and π_{RL} (Chen et al., 2025a) successfully integrate GRPO and other RL

paradigms into VLA refinement. However, a fundamental bottleneck remains: real-world RL necessitates intensive human intervention for resets and feedback, making it impractical for large-scale deployment. Even recent efforts like $\pi_{0.6}$ (Intelligence et al., 2025) remain prohibitively expensive in real-world settings. To address this, our framework eliminates the costs of physical interaction by simulating the real-world environment within a high-fidelity video world model, enabling efficient policy RL.

2.2. Robotic World Models

With recent advances in video generation (Wan et al., 2025; Blattmann et al., 2023), controllable video-based world models have become increasingly feasible. Unlike standard generative models that rely solely on text prompts, world models incorporate action sequences as conditioning signals. Many works in this direction leverage the strong spatiotemporal priors of large pretrained video models to enable action-conditioned simulation in domains such as gaming (Bruce et al., 2024; Yu et al., 2025) and autonomous driving (Ni et al., 2025; Hu et al., 2024), demonstrating promising performance.

More recently, driven by the rise of embodied AI, researchers have begun developing video world models conditioned on continuous robot actions. Several studies (Li et al., 2025a; Xiao et al., 2025; Quevedo et al., 2025; Ali et al., 2025; Zhang et al., 2025; Zhu et al., 2025) explore generating realistic robot execution videos from action sequences. However, existing world models often rely on external VLMs or heuristic proxy rewards, which lack the precision required for stable RL. And we also observe that most current models exhibit poor action-following accuracy and fail to reliably reflect true execution boundaries. A parallel line of work (Li et al., 2025c), exemplified by Cosmos Policy (Kim et al., 2026), pursues a unified approach by jointly predicting actions and future video frames. While these unified models exhibit high visual fidelity, they are primarily designed for imitation learning or zero-shot execution and lack the capability to function as interactive environments for RL. Our framework, World-VLA-Loop, addresses these limitations through a state-aware world model design and a co-evolving paradigm that enables more accurate action following and reward reliability.

Another direction within robotic world models is reconstructing the environment using point clouds (Allshire et al., 2025) or Gaussian Splatting (Lu et al., 2025b; Xia et al., 2025; Jain et al., 2025). While these methods achieve high accuracy in rendering precise spatial positions, a major weakness is that 3D-reconstructed worlds often fail to generalize to out-of-distribution cases; this includes not only regions uncaptured by the cameras but also complex physical dynamics. This limitation hinders the random exploration of

VLA policies within such world models—a process fundamental to achieving performance gains during RL training.

3. Method

As illustrated in Figure 3, our framework consists of four phases. First, we collect a large-scale dataset containing both success and near-success trajectories on various tasks spanning diverse execution outcomes. Next, we train an action-conditioned video world model with reward supervision on top of Cosmos-Predict (Ali et al., 2025) using this comprehensive dataset. Once trained, the model can be efficiently adapted to new, unseen scenarios using a few success and near-success demonstrations. The resulting fine-tuned model serves as a faithful virtual environment for robot policy evaluation and RL post-training, and the policy rollouts in real-world can also be fed back to augment the training dataset. In this section, we will introduce each stage in details.

3.1. Success and Near-Success Dataset

Existing open robotic datasets with action-trajectory annotations, regardless of their diversity, predominantly focus on successful executions as they are primarily curated for imitation learning. This convention restricts the diversity required to train robust world models, which consequently struggle to simulate physically plausible outcomes across diverse failure modes. While recent works like RoboFAC (Lu et al., 2025c) and AHA (Duan et al., 2024) have begun exploring failure data, they are designed for QA-style reasoning and lack action annotations. Moreover, these datasets are largely confined to simulation, leaving its practical utility underexplored.

In this paper, we introduce the Success and Near-Success Dataset (SANS), which leverages trajectories that nearly accomplish the target goal or sub-goal but fail due to minor inaccuracies in end-effector positioning. Such data is critical for training robust world models for two reasons: (1) because these trajectories are difficult to distinguish from successful executions, they force the world model to focus on fine-grained nuances in spatial dynamics; and (2) since robot policies frequently exhibit these “near-success” behaviors, including them ensures the virtual environment more accurately reflects the actual failure modes encountered during policy rollouts. We curate the SANS dataset across ManiSkill (Tao et al., 2024), LIBERO (Liu et al., 2023), and our own real-world robotic settings.

For the Maniskill (Tao et al., 2024) environment, we first craft simple control policies using ground-truth object poses to collect success trajectories and generate failure cases by perturbing these poses. Another approach is to collect failure trajectories directly from policy rollouts, capturing

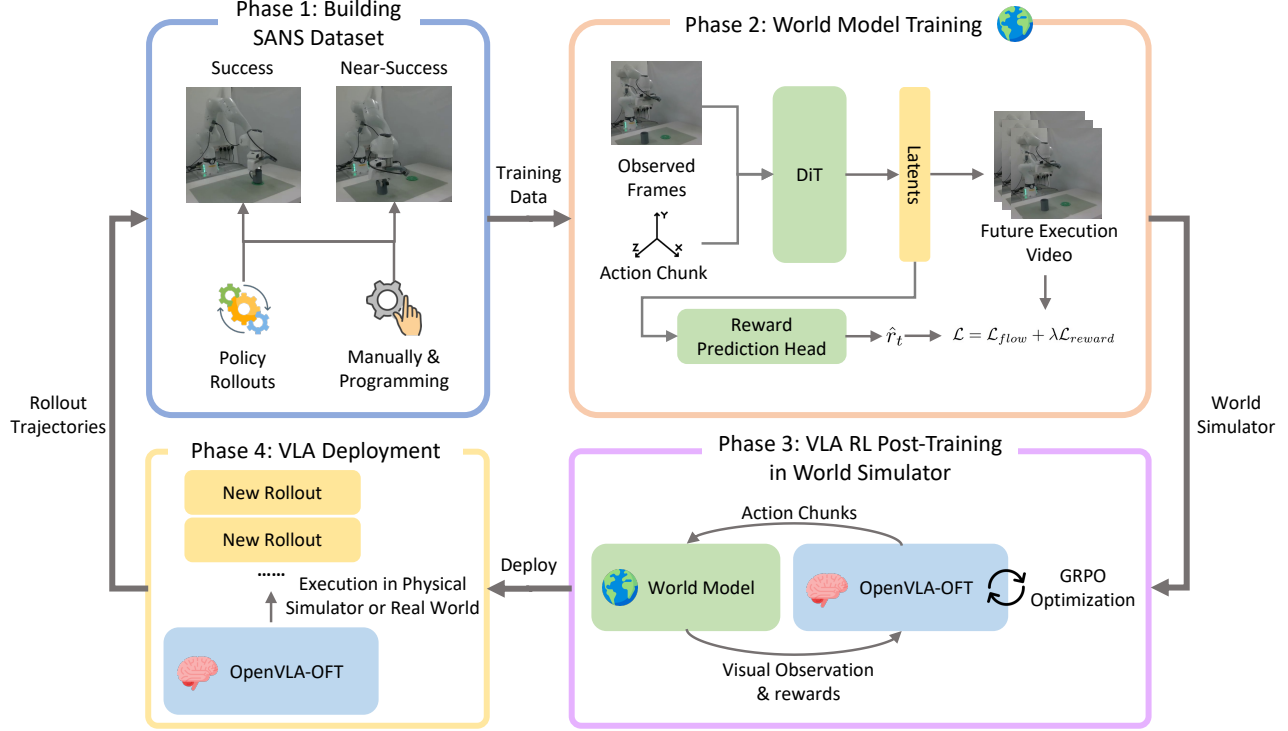


Figure 3. Full pipeline of our proposed framework. The process comprises four phases: (1) Curating the SANS dataset via manual teleoperation and policy rollouts; (2) Pretraining the action-conditioned world model on SANS with joint reward and video supervision; (3) Executing VLA policy rollouts within the world model to perform GRPO optimization; and (4) Deploying the refined policy to collect new failure and success data for further SANS augmentation. This cycle enables the joint optimization of the world model and the VLA policy, iteratively enhancing both performance.

natural failure modes that arise during execution. We follow this strategy for the LIBERO environment, using OpenVLA-OFT (Kim et al., 2025) to collect failure rollouts. Similarly, we collect data in real-world robotic settings by both manually teleoperating the robot to obtain plausible failure cases, and using fine-tuned OpenVLA-OFT policy to record their failure trajectories. In addition to the videos and actions, we also record the sparse reward signals at each execution step (binary values indicating whether the current state is a success state).

We first collect a large dataset on Maniskill for action-conditioned world model pretraining. In total, we have gathered approximately 35k video-action pairs spanning 23 different tasks, including both successful and various failure outcomes, which we use to pretrain our video world model. Additionally, we collect SANS dataset on LIBERO and in real scenarios, albeit in smaller quantities (roughly 50 failure trajectories and 50 success trajectories per task). We will demonstrate that our pretrained model can be efficiently fine-tuned and transferred to these unseen tasks.

3.2. State-aware Video World Simulator

We build our video world model on top of Cosmos-Predict 2 (Ali et al., 2025). Cosmos-Predict 2 is pretrained on a large corpus of embodiment-related video data and can be further adapted to incorporate robot action conditions. Given the first h observed frames x_0, \dots, x_{h-1} and next T timesteps of robot actions $a_1, \dots, a_T \in \mathbb{R}^6 \cup \{0, 1\}$ (represented as 6-DoF end-effector poses together with the gripper open/close state) the model synthesizes future execution frames for the next T steps, denoted as x_h, \dots, x_{h+T-1} .

Cosmos-Predict 2 utilizes a Diffusion Transformer (DiT) backbone to predict future video chunks autoregressively. To accommodate the action modality, an action embedder MLP maps each input pose into a latent tensor. These action embeddings are integrated into the DiT modules by adding them directly to the diffusion timestamp embeddings. This design enables the model to effectively ground its visual predictions in the provided control sequence while leveraging its strong pretrained generative priors.

To enable reward prediction without relying on external reward models, we augment the original generative model with a reward prediction head, as illustrated in Figure 3. After the DiT model produces diffusion latents, we add a

projection layer that maps these latents to a sequence of reward values, supervised by ground-truth rewards collected in the SANS dataset. Specifically, for each sampled timestep t , let z_t denote the denoised latent at the final step. The reward head ϕ predicts the scalar reward $\hat{r}_t = \phi(z_t)$, where ϕ is implemented as a lightweight MLP. During training, we jointly optimize the reward prediction head alongside the original flow matching loss (Lipman et al., 2022):

$$\mathcal{L} = \mathcal{L}_{flow} + \lambda \sum_{t=1}^T \|\hat{r}_t - r_t\|^2,$$

where the weighting factor λ is modulated according to the sampled noise level following the EDM framework (Karras et al., 2022). This ensures the reward head remains robust to the high-variance latents encountered during the early stages of the denoising process.

This design brings two key advantages. First, it provides a reliable reward generation mechanism within the world model. Since rewards are predicted based on the generated video latent states, they are intrinsically aligned with the actual visual outcomes and tend to be more accurate than low-level heuristic proxies or external VLM-based reward models. Second, joint training of the reward head and the video model encourages the generator to better distinguish successful versus failed execution outcomes under different action conditions. This leads to more accurate future video predictions—a crucial capability often lacking in existing video world models.

In practice, we first transfer the model from Cosmos-Predict original checkpoint to the collected Maniskill SANS dataset, and then fine-tune it to efficiently adapt to new scenarios using much less demonstrations, which also include both success and near-success trajectories. The Maniskill-pretrained model already possesses strong understanding and adherence to robot action conditions; the finetuning data further enables it to acquire knowledge of new environments, object textures, and task-specific physical interactions.

3.3. World Simulator for Policy RL Post-Training

Once trained to precisely generate execution outcomes conditioned on action inputs, our video world model serves as a reliable virtual environment for downstream policy evaluation and RL post-training.

We employ OpenVLA-OFT (Kim et al., 2025) as our base VLA model and adopt the training framework established by SimpleVLA-RL (Li et al., 2025b). For a target task characterized by a sparse SANS dataset (typically comprising fewer than 50 success and 50 near-success samples), we first fine-tune both the world model and the policy model to adapt to the specific scenario. Subsequently, we replace the conventional physics-based simulator in the SimpleVLA-RL

pipeline with our learned world model.

In this configuration, the world model generates next-step observations autoregressively based on the policy’s action outputs, which are then fed back to the policy for subsequent chunk predictions. This closed-loop interaction enables the policy to perform complete, multi-step rollouts within the world simulator. Furthermore, our world model provides a reward prediction at each step, which serves to determine the status of the current rollout. Following the SimpleVLA-RL protocol, after generating a group of rollouts within the world model, the VLA policy is updated via computed advantages.

As depicted in Figure 3, a key advantage of our method is the establishment of a comprehensive, iterative joint-optimization framework for both the world model and the VLA policy. Following each RL update, we collect success and near-success rollouts generated by the newly trained VLA policy when deployed in its target environment. These rollouts are then used to augment the SANS dataset for subsequent iterations of world model fine-tuning. This iterative refinement ensures that the world model progressively improves its ability to synthesize precise execution outcomes, which in turn enhances the effectiveness of the next RL phase for the VLA policy. In the experimental section, we validate that this joint-optimization process does yield superior VLA RL performance.

4. Experiments

The following section evaluates our framework across multiple dimensions, validating the effectiveness and broader applicability of the proposed approach. Our results demonstrate that: (1) The world model achieves an average visual alignment of 87.9% and a reward alignment of 86.4%, establishing it as a high-fidelity simulator for VLA policy rollouts. (2) Through RL post-training within our simulator, the OpenVLA-OFT policy achieves an average success rate improvement of 12.7% on the LIBERO benchmarks and 23.4% in real-world scenarios. (3) The proposed iterative refinement process further increases real-world task accuracy by 13.3% relative to the first RL checkpoint, underscoring the efficacy of the joint optimization cycle.

4.1. Experiment Settings

Experiment Scenarios. We conduct experiments on the LIBERO benchmark for simulated tasks, complemented by a self-constructed laboratory setup to evaluate real-world applicability. In both settings, the configuration consists of a Franka research arm (Haddadin et al., 2022) and a single third-person-view RealSense D435 camera (Keselman et al., 2017) mounted on a fixed position to provide observation input. For the real-world experiments, the robot control

system operates at a frequency of 10 Hz during both the data collection and deployment phases. We use a unified chunk size of 24 for all tasks in simulation and real-world. For more implementation details, please refer to Appendix A.

Evaluation Methods. We evaluate our pipeline through a hierarchical framework. First, we assess the generative performance of the World-VLA-Loop world model, focusing on visual fidelity and action-following precision. Building upon this, we quantify the model’s utility as a simulator by measuring the success rate improvements of a VLA policy during RL post-training.

4.2. World Model Evaluation

To ensure that the world model provides reliable generation suitable for accurate policy rollouts, we first evaluate its generative quality. Specifically, given a test dataset of image-actions pairs, the world model takes an initial image and a sequence of absolute robot end-effector poses as input. It then autoregressively predicts the video frames corresponding to the execution of those actions. We evaluate the resulting generations based on two primary dimensions: video quality and action-following accuracy.

Video Quality Since the generated frames serve as the major visual observations for the policy, in order to maintain the stable behavior of VLA, ensuring high visual fidelity is crucial. As indicated in Table 1, World-VLA-Loop world model achieves high-quality generation results across both simulation and real-world scenarios, yielding high-fidelity results with negligible structural and perceptual distortion. The consistency between the LIBERO and real-world metrics demonstrates that our world model generalizes effectively across different environments, providing a reliable visual foundation for downstream policy rollouts.

Table 1. Video generation performance. \uparrow indicates higher is better; \downarrow indicates lower is better.

Scenario	SSIM \uparrow	PSNR \uparrow	LPIPS \downarrow	MSE \downarrow
LIBERO	0.90	26.57	0.031	0.0024
Real-World	0.91	29.61	0.059	0.0019
Average	0.91	28.09	0.045	0.0022

Generation Accuracy A critical requirement for a world simulator is the ability to faithfully reflect the causal consequences of an action trajectory. While pixel-level metrics like MSE provide a baseline, a more robust evaluation measures the alignment between generated and ground-truth outcomes. To this end, we categorize the final state of each trajectory as either a success or failure and calculate the alignment rate—the percentage of samples where the predicted outcome matches the ground truth. Since our world model simultaneously generates video frames and scalar rewards, we report two distinct alignment metrics:

- *Visual Alignment*: This measures the faithfulness of the pixel-level generation. Success or failure is determined by evaluating the final generated video frames to judge the task outcome.
- *Reward Alignment*: This measures the accuracy of the world model’s internal reward head. A predicted trajectory is classified as a success if the generated reward exceeds a threshold of 0.9.

As shown in Table 2, our method effectively distinguishes between successful and failed trajectories across both LIBERO and real-world scenarios, achieving an average alignment accuracy exceeding 80% for both metrics. Furthermore, the outcomes classified via reward alignment are highly consistent with those from visual alignment. This strong correlation underscores the reliability of the internal reward prediction head and demonstrates that its learned success criteria are well-aligned with human judgment.

4.3. World Simulator for VLA Post-training

Basic RL Training Leveraging its reliable generative performance, World-VLA-Loop world model serves as a learned simulator for VLA policy post-training. For each task, we first conduct task-specific finetuning for both the OpenVLA policy and the world model. Subsequently, the policy is deployed within the world model environment for RL post-training. We adopt the RL pipeline from SimpleVLA-RL (Li et al., 2025b), adapting the rollout process to operate entirely within our neural simulator. In this configuration, only the initial frame is sourced from the original dataset; all subsequent observations are autoregressively generated by the world model conditioned by the policy’s predicted actions. Finally, the RL reward is derived from the world model’s reward head, utilizing a thresholding mechanism to determine the binary success signals required for group relative optimization (Shao et al., 2024).

We conduct experiments across three task suites from the LIBERO benchmark and task in a real-world setting. Since LIBERO-100 primarily involves long-horizon tasks requiring the generation of over 200 video frames, where current autoregressive video models often suffer from severe quality drift, we leave its exploration for future work. For each task, 80–100 success and near-success trajectories are utilized to fine-tune the world model; among these, a subset of approximately 50 success trajectories is used to fine-tune the OpenVLA policy. As illustrated in Table 3 and Figure 4, success rates across both the LIBERO suites and the real-world task exhibit significant improvements throughout the RL post-training process. To clarify, the real-world success rate curves in Figure 4 are evaluated within the world simulator, whereas the final results reported in Table 3 are obtained through physical, real-world experiments.

Iterative Refinement through Policy Rollouts As dis-

Table 2. Outcome Alignment Performance across specific LIBERO and Real-World tasks. For each task we evaluate 20 samples within validation set, and report the percentage of samples where the predicted success/failure matches the ground truth.

Metric	LIBERO-Object		LIBERO-Goal		LIBERO-Spatial		Real-World
	Task 1	Task 2	Task 1	Task 2	Task 1	Task 2	
World-VLA-Loop Visual Alignment	85%	95%	90%	75%	85%	95%	90%
World-VLA-Loop Reward Alignment	75%	90%	85%	75%	90%	95%	95%

Table 3. Success rate of OpenVLA-OFT before and after RL training. Success rates are computed across 500 rollouts for the LIBERO suites and 30 physical rollouts for our real-world experiments.

Model	LIBERO-Object		LIBERO-Goal		LIBERO-Spatial		Real-World
	Task 1	Task 2	Task 1	Task 2	Task 1	Task 2	
SFT Base	73.9%	73.9%	91.9%	86.1%	83.9%	87.9%	13.3%
RL Post-Training (World-VLA-Loop)	97.9%	91.9%	100%	96.2%	93.9%	94.0%	36.7%
Δ vs SFT	+24.0%	+18.0%	+8.1%	+10.1%	+10.0%	+6.1%	+23.4%

cussed in Section 3.3, once a functional policy is established, its generated trajectories can be leveraged to augment the SANS dataset. This augmented data is then utilized to further refine the world model, enhancing its precision and action-following capabilities. Ultimately, this iterative cycle improves the overall efficiency of VLA reinforcement learning within the neural simulator.

We conduct iterative experiments within our real-world setting. In the initial phase (Step 0), the SUPA dataset comprises manually collected success and near-success trajectories, alongside rollouts from the SFT OpenVLA-OFT baseline. For the next iteration (Step 1), the dataset is expanded to include newly generated trajectories from the RL-optimized policy produced in the previous step. Both world models are initialized from the ManiSkill-pretrained checkpoint, while the VLA policies for each RL stage begin from the base SFT version. As illustrated in Figure 1 (b), this iterative refinement successfully boosts performance: the base SFT policy achieved only a 13.3% success rate, which is increased by 23.4% in the first RL stage, and eventually reached 50.0% in the second iteration. These results demonstrate the overall effectiveness of our proposed closed-loop framework in enabling continuous policy and world model improvement.

4.4. Ablation Study

Reward Prediction Head We conduct ablation experiments to validate the effectiveness of the reward prediction head. First, we examine the world model’s performance after removing this head. As indicated in Table 4, visual alignment drops by approximately 30% without reward supervision, suggesting that joint training of the reward head and the diffusion backbone significantly improves the model’s ability

Table 4. Ablation results. We investigate how different design choices influence the world model prediction accuracy.

Metric	LIBERO-Object	
	Task 1	Task 2
Visual Alignment (w/o near-success data)	60%	65%
Visual Alignment (w/o reward prediction head)	60%	70%
Reward Alignment (Qwen3-VL)	50%	55%
Visual Alignment (ours)	85%	95%
Reward Alignment (ours)	75%	90%

to discriminate between different action outcomes. Second, we compare our reward head against Qwen3-VL (Bai et al., 2025) acting as a success-failure judge—a common approach in prior literature. Specifically, we provide Qwen3-VL with the video frames generated by our world model and prompt it to evaluate the task’s final success status. Notably, these are the same frames used to produce our internal reward predictions. The results in Table 4 show that the VLM suffers from severe hallucination, making it a less reliable reward function for RL compared to our method. While task-specific fine-tuning might improve VLM accuracy, it would significantly increase pipeline complexity. In contrast, our reward prediction head, which shares the backbone with the video generator, is not only more accurate but also enhances video quality through the benefits of joint training. For more results please refer to Appendix B.

Near-Success Data during World Model Training We also fine-tune the world model while excluding near-success

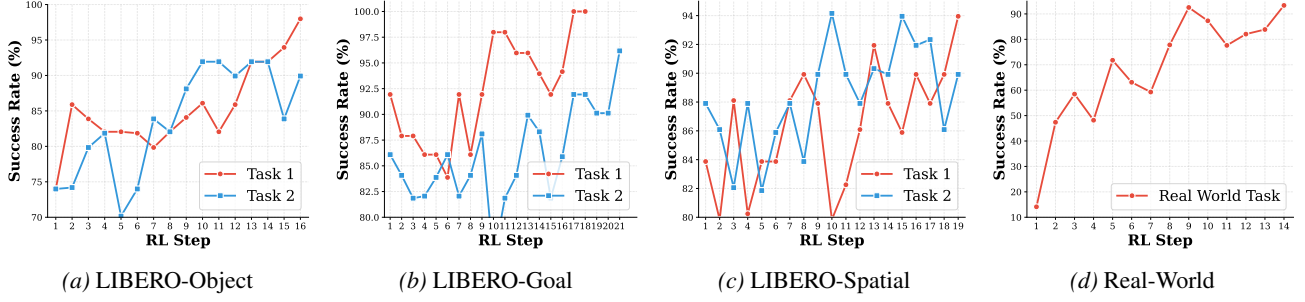


Figure 4. Success rate improvements along World-VLA-Loop RL training steps.

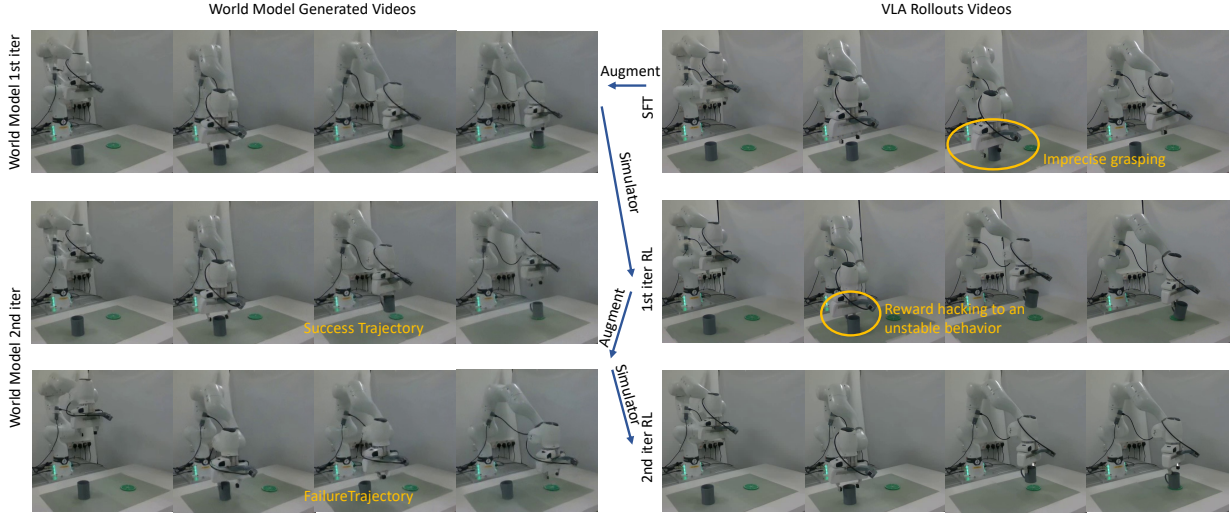


Figure 5. Examples of world model generated rollouts and actual execution videos by both SFT policy and RL post-trained policy.

trajectories. As indicated in Table 4, the visual alignment of the generated videos decreases significantly under this configuration. This confirms that near-success trajectories are indispensable for world model training, as they enable the model to internalize potential failure modes possible during VLA execution and more faithfully reflect resulting action outcomes.

4.5. Qualitative Results

Figure 5 presents qualitative examples of synthesized world model rollouts alongside actual VLA policy executions. Through our iterative refinement loop, the world model progressively learns to cover a broader action space and better represent the stochasticity of VLA exploration. In the policy rollouts, we observe that the SFT-baseline tends to generate imprecise grasping poses. While the first RL iteration mitigates this issue, the policy initially engages in reward hacking, converging on suboptimal grasps such as the back of the mug, since the first iteration world model fails to accurately model the physical consequences of such interactions. After augmenting the SANS dataset, the world model develops a finer awareness of these edge cases. Consequently, the

VLA policy trained within this refined environment achieves significantly more precise and robust grasping poses. For additional qualitative examples, please refer to Appendix C.

Notably, our world model demonstrates the ability to synthesize trajectories unseen during the fine-tuning of the target SANS dataset, leveraging the broad priors learned during its pretraining on ManiSkill. Figure 6 illustrates cases where the world model is conditioned on entirely novel action sequences and robot arm trajectories. Despite the stochastic nature of these out-of-distribution inputs, the model faithfully adheres to the action conditioning, generating physically plausible motion aligning with ground truth. This robustness indicates that the world model has effectively internalized the underlying mapping between control actions and robotic kinematics, rather than merely memorizing training sequences.

5. Conclusion

We presented World-VLA-Loop, a novel framework for world-model-based VLA reinforcement learning through the joint optimization of our world model and VLA policy.

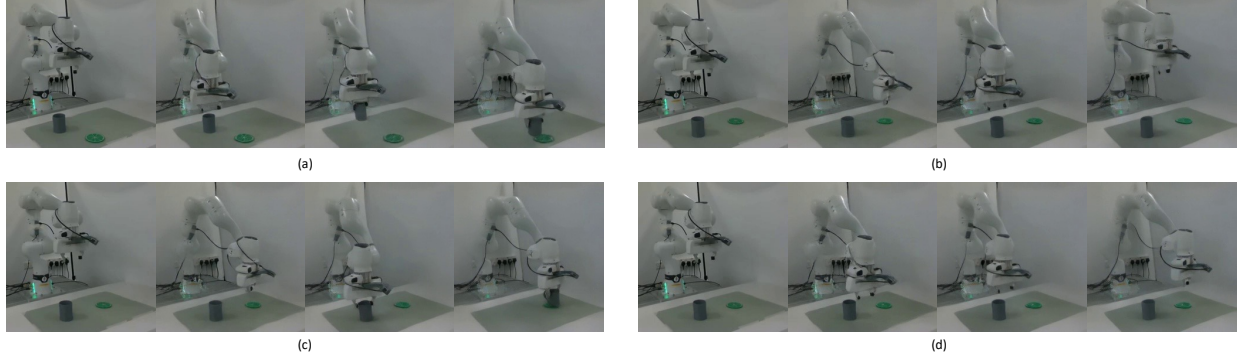


Figure 6. World model generation results on unseen action sequences. (a) The plate is initialized directly in front of the mug. (b) The gripper moves to the right, returns to the mug’s overhead position, and retracts to a neutral pose. (c) The gripper first moves to the right, followed by a successful pick-and-place of the mug onto the plate. (d) A sequence of forward, backward, and lateral oscillations.

By leveraging the SANS dataset curated with near-success trajectories, we trained a high-fidelity world model with integrated reward supervision, enabling effective policy refinement within a virtual environment. Furthermore, our co-evolving paradigm uses real-world rollouts to augment training data, progressively enhancing both world model grounding and policy performance. Experiments demonstrate significant success rate gains across simulation and real-world benchmarks, offering a scalable direction for real-world RL by reducing reliance on costly physical interactions.

Limitations and Future Work: Current autoregressive video models suffer from limited context memory and quality drift, which diminishes performance in long-horizon tasks exceeding 200 frames (or approximately 20 seconds of video). Future research will explore integrating video backbones with enhanced long-term stability. Additionally, transitioning from sparse final-state rewards to step-wise intermediate sub-goals could further improve reward head accuracy and RL convergence.

Impact Statement

This paper presents work whose goal is to advance the field of Robot Learning. It aims at solving difficult real-world reinforcement learning of robot policy, providing an alternative approach for on-policy VLA RL.

Author Contribution Statements

Xiaokang Liu and Hai Ci conceptualized the project. Xiaokang Liu designed the world model, conducted the primary experiments, and wrote the manuscript. Zechen Bai implemented the VLA RL paradigm, integrated the world model into the RL pipeline, and executed the RL training experiments. Hai Ci coordinated the project, provided key technical insights, and led team discussions. Kevin Yuchen

Ma established the robotic environments and hardware configurations.

References

Ali, A., Bai, J., Bala, M., Balaji, Y., Blakeman, A., Cai, T., Cao, J., Cao, T., Cha, E., Chao, Y.-W., et al. World simulation with video foundation models for physical ai. *arXiv preprint arXiv:2511.00062*, 2025.

Allshire, A., Choi, H., Zhang, J., McAllister, D., Zhang, A., Kim, C. M., Darrell, T., Abbeel, P., Malik, J., and Kanazawa, A. Visual imitation enables contextual humanoid control. *arXiv preprint arXiv:2505.03729*, 2025.

Bai, S., Cai, Y., Chen, R., Chen, K., Chen, X., Cheng, Z., Deng, L., Ding, W., Gao, C., Ge, C., Ge, W., Guo, Z., Huang, Q., Huang, J., Huang, F., Hui, B., Jiang, S., Li, Z., Li, M., Li, M., Li, K., Lin, Z., Lin, J., Liu, X., Liu, J., Liu, C., Liu, Y., Liu, D., Liu, S., Lu, D., Luo, R., Lv, C., Men, R., Meng, L., Ren, X., Ren, X., Song, S., Sun, Y., Tang, J., Tu, J., Wan, J., Wang, P., Wang, P., Wang, Q., Wang, Y., Xie, T., Xu, Y., Xu, H., Xu, J., Yang, Z., Yang, M., Yang, J., Yang, A., Yu, B., Zhang, F., Zhang, H., Zhang, X., Zheng, B., Zhong, H., Zhou, J., Zhou, F., Zhou, J., Zhu, Y., and Zhu, K. Qwen3-vl technical report. *arXiv preprint arXiv:2511.21631*, 2025.

Black, K., Brown, N., Driess, D., Esmail, A., Equi, M., Finn, C., Fusai, N., Groom, L., Hausman, K., Ichter, B., et al. π_0 : A vision-language-action flow model for general robot control. *arXiv preprint arXiv:2410.24164*, 2024.

Blattmann, A., Dockhorn, T., Kulal, S., Mendelevitch, D., Kilian, M., Lorenz, D., Levi, Y., English, Z., Voleti, V., Letts, A., et al. Stable video diffusion: Scaling latent video diffusion models to large datasets. *arXiv preprint arXiv:2311.15127*, 2023.

Bruce, J., Dennis, M. D., Edwards, A., Parker-Holder, J., Shi, Y., Hughes, E., Lai, M., Mavalankar, A., Steigerwald, R., Apps, C., et al. Genie: Generative interactive environments. In *Forty-first International Conference on Machine Learning*, 2024.

Chen, K., Liu, Z., Zhang, T., Guo, Z., Xu, S., Lin, H., Zang, H., Li, X., Zhang, Q., Yu, Z., et al. π_{RL} : Online rl fine-tuning for flow-based vision-language-action models. *arXiv preprint arXiv:2510.25889*, 2025a.

Chen, T., Chen, Z., Chen, B., Cai, Z., Liu, Y., Li, Z., Liang, Q., Lin, X., Ge, Y., Gu, Z., et al. Robotwin 2.0: A scalable data generator and benchmark with strong domain randomization for robust bimanual robotic manipulation. *arXiv preprint arXiv:2506.18088*, 2025b.

Driess, D., Xia, F., Sajjadi, M. S., Lynch, C., Chowdhery, A., Wahid, A., Tompson, J., Vuong, Q., Yu, T., Huang, W., et al. Palm-e: An embodied multimodal language model. 2023.

Duan, J., Pumacay, W., Kumar, N., Wang, Y. R., Tian, S., Yuan, W., Krishna, R., Fox, D., Mandlekar, A., and Guo, Y. Aha: A vision-language-model for detecting and reasoning over failures in robotic manipulation. *arXiv preprint arXiv:2410.00371*, 2024.

Haddadin, S., Parusel, S., Johannsmeier, L., Golz, S., Gabl, S., Walch, F., Sabaghian, M., Jähne, C., Hausperger, L., and Haddadin, S. The franka emika robot: A reference platform for robotics research and education. *IEEE Robotics & Automation Magazine*, 29(2):46–64, 2022. doi: 10.1109/MRA.2021.3138382.

Hu, X., Yin, W., Jia, M., Deng, J., Guo, X., Zhang, Q., Long, X., and Tan, P. Drivingworld: Constructing world model for autonomous driving via video gpt. *arXiv preprint arXiv:2412.19505*, 2024.

Intelligence, P., Amin, A., Aniceto, R., Balakrishna, A., Black, K., Conley, K., Connors, G., Darpinian, J., Dhabalia, K., DiCarlo, J., et al. $\pi_{0.6}$: a vla that learns from experience. *arXiv preprint arXiv:2511.14759*, 2025.

Jain, A., Zhang, M., Arora, K., Chen, W., Torne, M., Irshad, M. Z., Zakharov, S., Wang, Y., Levine, S., Finn, C., et al. Polaris: Scalable real-to-sim evaluations for generalist robot policies. *arXiv preprint arXiv:2512.16881*, 2025.

Karamchetti, S., Nair, S., Balakrishna, A., Liang, P., Kollar, T., and Sadigh, D. Prismatic vlms: Investigating the design space of visually-conditioned language models. In *Forty-first International Conference on Machine Learning*, 2024.

Karras, T., Aittala, M., Aila, T., and Laine, S. Elucidating the design space of diffusion-based generative models. *Advances in neural information processing systems*, 35: 26565–26577, 2022.

Keselman, L., Iselin Woodfill, J., Grunnet-Jepsen, A., and Bhowmik, A. Intel realsense stereoscopic depth cameras. In *Proceedings of the IEEE conference on computer vision and pattern recognition workshops*, pp. 1–10, 2017.

Kim, M. J., Pertsch, K., Karamchetti, S., Xiao, T., Balakrishna, A., Nair, S., Rafailov, R., Foster, E., Lam, G., Sanketi, P., et al. Openvla: An open-source vision-language-action model. *arXiv preprint arXiv:2406.09246*, 2024.

Kim, M. J., Finn, C., and Liang, P. Fine-tuning vision-language-action models: Optimizing speed and success. *arXiv preprint arXiv:2502.19645*, 2025.

Kim, M. J., Gao, Y., Lin, T.-Y., Lin, Y.-C., Ge, Y., Lam, G., Liang, P., Song, S., Liu, M.-Y., Finn, C., et al. Cosmos policy: Fine-tuning video models for visuomotor control and planning. *arXiv preprint arXiv:2601.16163*, 2026.

Li, H., Ding, P., Suo, R., Wang, Y., Ge, Z., Zang, D., Yu, K., Sun, M., Zhang, H., Wang, D., et al. Vla-rft: Vision-language-action reinforcement fine-tuning with verified rewards in world simulators. *arXiv preprint arXiv:2510.00406*, 2025a.

Li, H., Zuo, Y., Yu, J., Zhang, Y., Yang, Z., Zhang, K., Zhu, X., Zhang, Y., Chen, T., Cui, G., et al. Simplevla-rl: Scaling vla training via reinforcement learning. *arXiv preprint arXiv:2509.09674*, 2025b.

Li, S., Gao, Y., Sadigh, D., and Song, S. Unified video action model. *arXiv preprint arXiv:2503.00200*, 2025c.

Lipman, Y., Chen, R. T., Ben-Hamu, H., Nickel, M., and Le, M. Flow matching for generative modeling. *arXiv preprint arXiv:2210.02747*, 2022.

Liu, B., Zhu, Y., Gao, C., Feng, Y., Liu, Q., Zhu, Y., and Stone, P. Libero: Benchmarking knowledge transfer for lifelong robot learning. *Advances in Neural Information Processing Systems*, 36:44776–44791, 2023.

Liu, X., Ma, K. Y., Gao, C., and Shou, M. Z. Diffusion models in robotics: A survey. 2025.

Lu, G., Guo, W., Zhang, C., Zhou, Y., Jiang, H., Gao, Z., Tang, Y., and Wang, Z. Vla-rl: Towards masterful and general robotic manipulation with scalable reinforcement learning. *arXiv preprint arXiv:2505.18719*, 2025a.

Lu, G., Jia, B., Li, P., Chen, Y., Wang, Z., Tang, Y., and Huang, S. Gwm: Towards scalable gaussian world models for robotic manipulation. In *Proceedings of the*

IEEE/CVF International Conference on Computer Vision,
pp. 9263–9274, 2025b.

Lu, W., Ye, M., Ye, Z., Tao, R., Yang, S., and Zhao, B. Robofac: A comprehensive framework for robotic failure analysis and correction. *arXiv preprint arXiv:2505.12224*, 2025c.

Ni, J., Guo, Y., Liu, Y., Chen, R., Lu, L., and Wu, Z. Maskgwm: A generalizable driving world model with video mask reconstruction. In *Proceedings of the Computer Vision and Pattern Recognition Conference*, pp. 22381–22391, 2025.

Quevedo, J., Liang, P., and Yang, S. Evaluating robot policies in a world model. *arXiv preprint arXiv:2506.00613*, 2025.

Shao, Z., Wang, P., Zhu, Q., Xu, R., Song, J., Bi, X., Zhang, H., Zhang, M., Li, Y., Wu, Y., et al. Deepseekmath: Pushing the limits of mathematical reasoning in open language models. *arXiv preprint arXiv:2402.03300*, 2024.

Tao, S., Xiang, F., Shukla, A., Qin, Y., Hinrichsen, X., Yuan, X., Bao, C., Lin, X., Liu, Y., Chan, T.-k., et al. Maniskill3: Gpu parallelized robotics simulation and rendering for generalizable embodied ai. *arXiv preprint arXiv:2410.00425*, 2024.

Wan, T., Wang, A., Ai, B., Wen, B., Mao, C., Xie, C.-W., Chen, D., Yu, F., Zhao, H., Yang, J., et al. Wan: Open and advanced large-scale video generative models. *arXiv preprint arXiv:2503.20314*, 2025.

Xia, H., Su, E., Memmel, M., Jain, A., Yu, R., Mbiziwo-Tiapo, N., Farhadi, A., Gupta, A., Wang, S., and Ma, W.-C. Drawer: Digital reconstruction and articulation with environment realism. In *Proceedings of the Computer Vision and Pattern Recognition Conference*, pp. 21771–21782, 2025.

Xiao, J., Yang, Y., Chang, X., Chen, R., Xiong, F., Xu, M., Zheng, W.-S., and Zhang, Q. World-env: Leveraging world model as a virtual environment for vla post-training. *arXiv preprint arXiv:2509.24948*, 2025.

Yu, J., Qin, Y., Wang, X., Wan, P., Zhang, D., and Liu, X. Gamefactory: Creating new games with generative interactive videos. *arXiv preprint arXiv:2501.08325*, 2025.

Zhang, J., Huang, Z., Gu, C., Ma, Z., and Zhang, L. Reinforcing action policies by prophesying. *arXiv preprint arXiv:2511.20633*, 2025.

Zhu, F., Yan, Z., Hong, Z., Shou, Q., Ma, X., and Guo, S. Wmpo: World model-based policy optimization for vision-language-action models. *arXiv preprint arXiv:2511.09515*, 2025.

A. Implementation Details

A.1. World Model Training

We transfer the world model from Cosmos Predict 2 action-conditioned version checkpoint. As stated in the main paper, we first train the world model on a collected Maniskill SANS dataset. This stage enables the model to grasp basic relationship between Franka robot arm and conditioning action, as well as some fundamental physics dynamics in manipulation scenarios. After this pretraining phase, we can adapt our model towards any downstream task with few data (less than 100 success and near-success trajectories). For the downstream task fine-tuning, we adopt a smaller learning rate and keep using full parameter tuning.

A.2. VLA Deployment in World Model

We adapt the SimpleVLA-RL codebase by replacing the physical simulator with our learned world model, while maintaining a consistent interface across both environments. To facilitate the batch optimization required for GRPO, we implement the interaction between the VLA policy and the world model via a request-response architecture. The world model operates as a backend server that monitors incoming requests; once the VLA policy generates an action chunk, it is transmitted to the server, which allocates the task to an available model worker to compute the subsequent observation and reward signals. Regarding efficiency, a batched generation of 24 video frames requires approximately 7 seconds on a NVIDIA H100 node. Given that SimpleVLA-RL typically converges within 50 optimization steps, we can finish RL training for one task in 30 hours.

B. Additional Ablation

Due to space constraints in Section 4.4, we provide a comprehensive ablation analysis of the reward prediction head in this section. As demonstrated in Table 5, the integration of the reward prediction head yields consistent performance gains across all tasks. This indicates that joint supervision—leveraging both sparse reward signals and dense video objectives—serves as a powerful regularizer, significantly enhancing the world model’s generation accuracy and grounding.

C. Visual Examples

We provide additional qualitative examples of our world model’s generation capabilities in this section. Figure 7 illustrates failure rollouts synthesized by the world model when conditioned on erroneous action trajectories. The generated video frames demonstrate that the world model accurately adheres to the conditioning actions and precisely distinguishes between nuanced outcomes resulting from in-

correct execution. This capability ensures that the model covers a diverse range of failure modes, providing the necessary grounding for effective policy refinement. Figure 8 provides some examples of generated successful trajectories. Most of the videos show that world model can clearly distinguish between failure and success action inputs.

Table 5. Full ablation results on reward prediction head.

Metric	LIBERO-Object		LIBERO-Goal		LIBERO-Spatial		Real-World
	Task 1	Task 2	Task 1	Task 2	Task 1	Task 2	
Visual Alignment (w/o reward prediction head)	60%	70%	85%	65%	80%	85%	85%
Visual Alignment	85%	95%	90%	75%	85%	95%	90%
Reward Alignment	75%	90%	85%	75%	90%	95%	95%

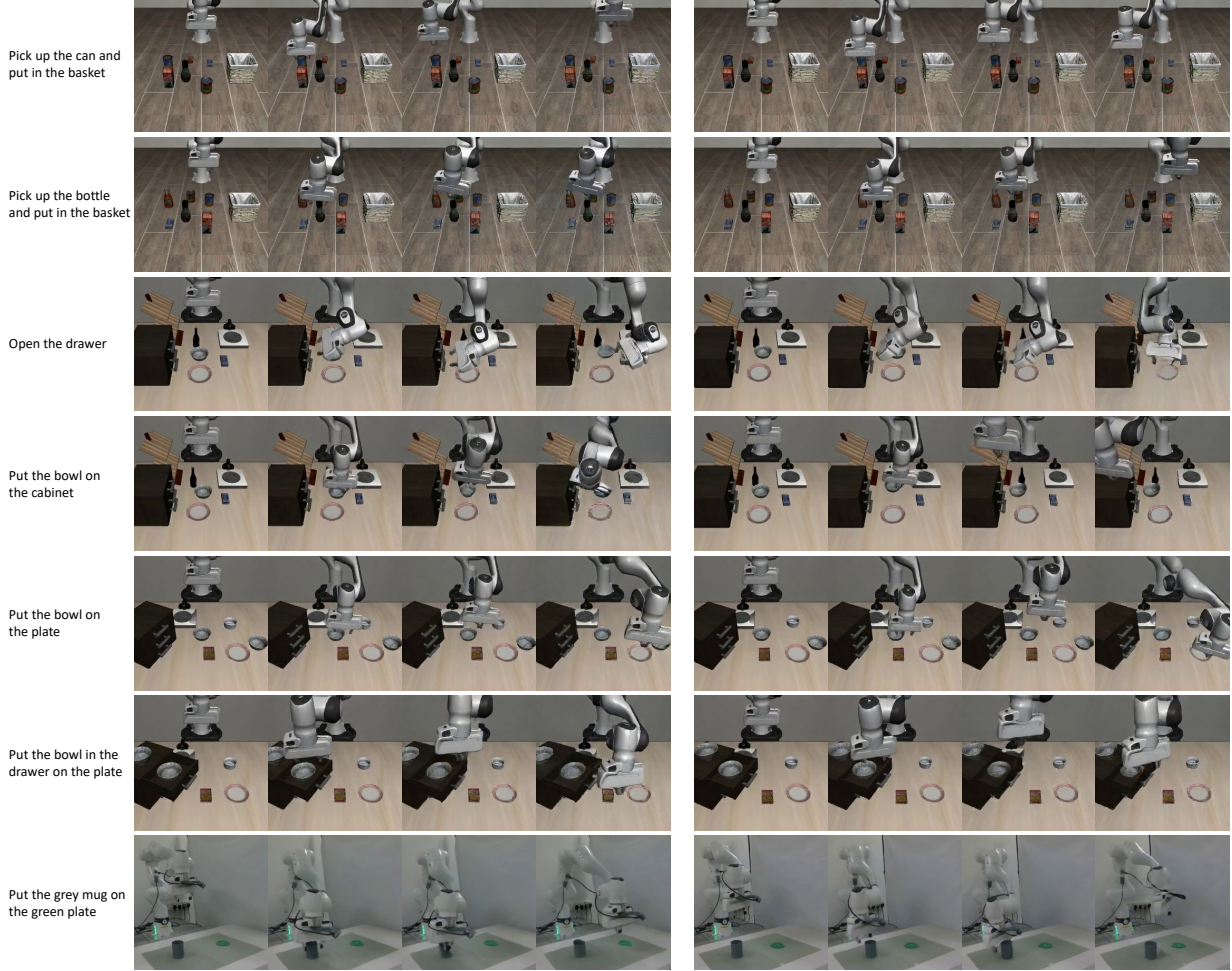


Figure 7. Examples of world model generated rollouts of failure trajectories.

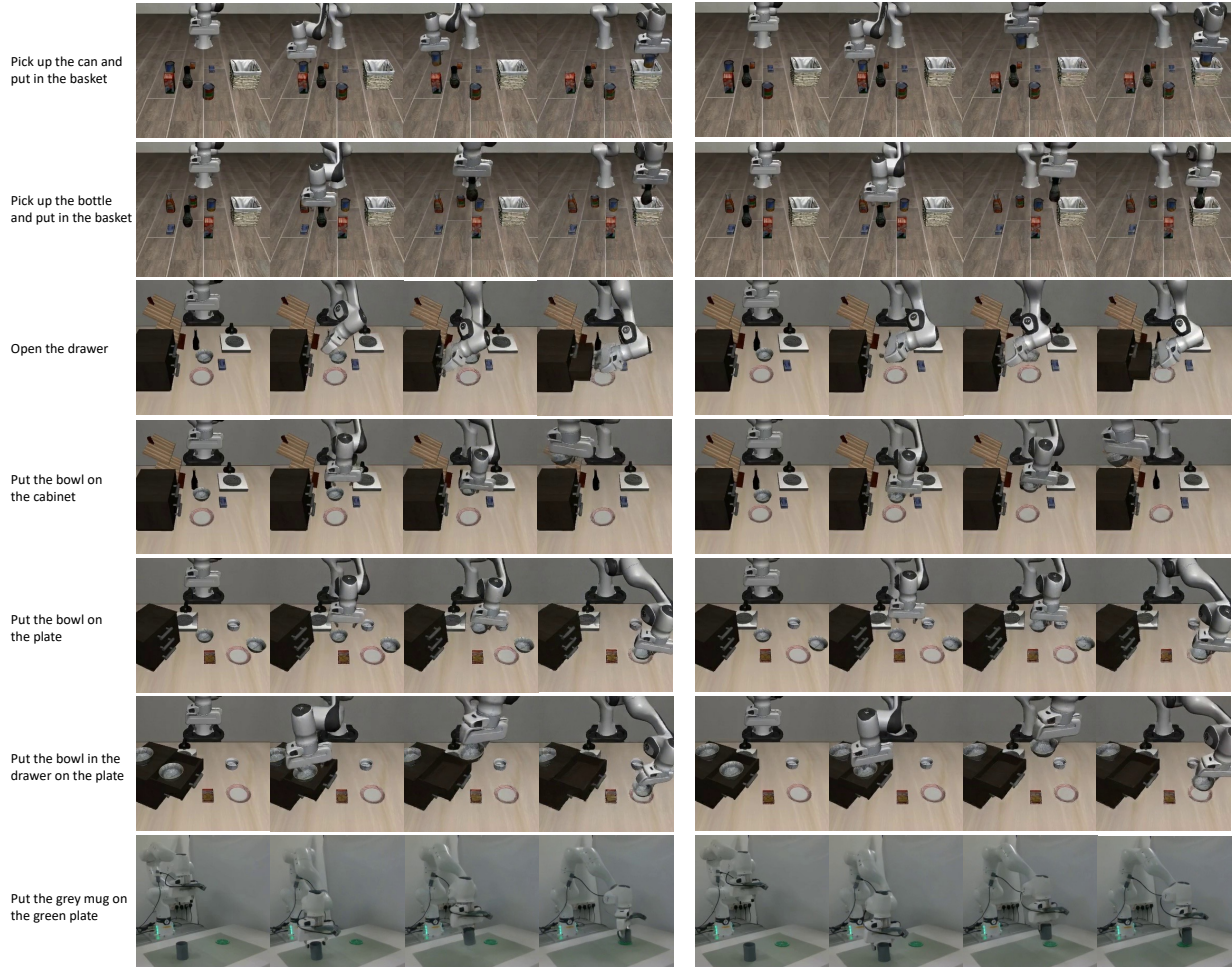


Figure 8. Examples of world model generated rollouts of successful trajectories.